Gell River Fire Driven by Forced Channeling and Lateral Fire in 2018–19 Summer, Tasmania

Mitsuhiro Ozaki * , Grant Williamson , Paul Fox-Hughes , Peter Love , Jagannath Aryal

Posted Date: 21 July 2023

doi: 10.20944/preprints202307.1502.v1

Keywords: Rugged terrain, AFDRS, buttongrass, forced channeling, lateral fire channeling

Article

Gell River Fire Driven by Forced Channeling and Lateral Fire in 2018–19 Summer, Tasmania

Mitsuhiro Ozaki [1,*], Grant Williamson [2], Paul Fox-Hughes [3], Peter Love [4] and Jagannath Aryal [5]

[1] School of Natural Sciences, University of Tasmania, Hobart, TAS 7005, Australia
[2] School of Natural Sciences, University of Tasmania, Hobart, TAS 7005, Australia; grant.williamson@utas.edu.au
[3] Research Program, Bureau of Meteorology, Hobart, TAS 7000, Australia paul.fox-hughes@bom.gov.au
[4] School of Geography, Planning, and Spatial Sciences, University of Tasmania, Sandy Bay, TAS 7005, Australia p.t.love@utas.edu.au
[5] Department of Infrastructure Engineering, Faculty of Engineering and IT, The University of Melbourne, Melbourne, VIC 3010, Australia; jagannath.aryal@unimelb.edu.au
* Correspondence: mitsuhiro.ozaki@utas.edu.au

Abstract. Mountain fire can become more complex than fires at lower elevation due to the complex interaction of fire, topography, and weather. The Gell River Fire in Tasmania, Australia occurred in rugged terrain where there are abundant fire sensitive vegetation communities, as well as the presence of infrastructure including high-voltage transmission lines. The fire began at the end of December 2018 and lasted a few months, with a final burnt area of approximately 350 km^2 despite significant fire suppression effort. The fire was investigated by employing wind vector maps, numerical weather model vertical sounding charts (NWMVS) and Prototype 2, which is an integrated fire simulator and can detect lateral fire channeling (LFC). Our analysis of the fire found its spread was likely to be introduced into a valley by forced channeling (FC), which is modified synoptic wind, and showed rapid spread in the valley. The simulated fire also showed wider spread than the observed data in the valley, with the simulated fire impacting highly sensitive vegetation communities on the fringes of the valley. This alludes to some potential conclusions: (1) The loss of fire sensitive vegetation would have increased if fire suppression activity had not been conducted. (2) Spotting fires could be produced by LFC because these spotting fire would allow spreading fire in a shorter period. (3) Heterogeneity of vegetation, such as combination of buttongrass and forest, could help carry fire rapidly in the valley with LFC. Fire can propagate faster in buttongrass than in forests while the forests allow the spotting fire.

Keywords: rugged terrain; AFDRS; buttongrass; forced channeling; lateral fire channeling

1. Introduction

Although wildfires are common in Australia, these events vary in frequency and intensity due to the various climates and topography throughout the country (Bradstock, 2010). In particular, fires in mountainous areas are fraught with difficulty in predicting fire behavior because of the interaction of complex topography, dynamic wind and fuels (Abouali et al., 2021; Edalati-nejad et al., 2021). Dynamic winds in the rugged terrain influence not only fire behavior but also cause smoke to disperse distantly (Heilman, 2023; J. Sharples et al., 2011). Mountain fires are common in Tasmania, which has formed rugged terrain due to past glacial or periglacial erosion (Bowman et al., 2022). For example, 36 individual fire events occurred and became larger fires such as at Great Pine Tier, Gell River, and Riveaux Road, each of which contains Tasmanian Wilderness World Heritage Area (TWWHA) in the summer between 2018 and 2019 (Australasian Fire and Emergency Service Authorities Council, 2019; Blackwood et al., 2023).

This paper studies the Gell River Fire which started on 28th December 2018 and burnt a total of 350 km^2(Land Information System Tasmania, 2020). The Gell River Fire site is poorly accessible due to remote rugged terrain and consists of variety of vegetation types. The dominant vegetation is

buttongrass moorland, which is highly flammable, can smolder and may also carry fires to more fire-sensitive vegetation (Marsden-Smedley et al., 2001; Storey, 2010). In addition, some of the vegetation in the area is ranked as extremely sensitive or highly sensitive to fire impact (Land Information System Tasmania, 2020). Although heterogeneity of vegetation is often considered as mitigating fire (Simeoni et al., 2011; Turner et al., 2009), buttongrass moorland can facilitate spreading fire in such susceptible other vegetation by lingering persistently in this study fire. After the ignition of the fire, fire crews reportedly left the fire site believing the fire had been sufficiently suppressed on December 31st, 2018. Contrary to expectations, the fire reemerged and propagated to the southeast in the following days (Australasian Fire and Emergency Service Authorities Council, 2019). In the vicinity of Gell River region, transmission lines linked to Gordon Power Station, which is the largest hydroelectric power station in Tasmania, were once threatened by the fire, yet the transmissions stayed intact (Australasian Fire and Emergency Service Authorities Council, 2019; Hydro Tasmania, n.d.).

In this analysis, we focus on two types of atypical winds and one fire phenomenon: forced channeling (FC) and downslope wind (DW) as well as lateral fire channeling (LFC). Forced channeling (FC) is often abrupt and occurs when the friction of geostrophic wind across a valley is greater than the friction along the valley axis (J. J. Sharples, 2009). It is more common during daytime than at night because the atmosphere is generally unstable during daytime due to the absence of nocturnal inversion, so that the geostrophic wind can influence the ground surface level. In particular, this dynamic wind favors late morning when the nocturnal inversion dissipates, and is prone to occur in small, narrow mountain passes or saddles (Kossmann et al., 2001; J. J. Sharples, 2009; Whiteman, 2000). The wind magnitude is generally the highest under neutral atmospheric conditions and when the wind aloft enters a valley directly along the valley linear to its axis (J. J. Sharples, 2009; Smedman et al., 1996; Whiteman, 2000). It is necessary to be cautious about the wind direction in anticipating fire spread because this wind can suddenly change by 180° when the wind aloft transverses across the valley axis (J. J. Sharples, 2009; Whiteman, 2000). Forced channeling (FC) requires downward transport of momentum and can be strengthened by the foehn effect in elevated areas (Whiteman, 2000). The second atypical wind type is downslope wind (DW) which often causes hazardous fire behavior to occur, even during prescribed fires in winter (J. J. Sharples, 2009). The sudden drop in dew point temperature, which is the temperature by which the water component in a given parcel is saturated at constant pressure (American Meteorological Society, 2020), can be an indicator of large-scale downslope wind (J. J. Sharples, 2009; J. J. Sharples et al., 2010). It is also possible for downslope wind to take place at lower altitude. For example, the Waroona Fire (2016) in Western Australia started by lightning at around 500 m elevation above mean sea level, and proceeded downhill rapidly, driven by downslope winds, and ended up burning approximately 700 km^2 (Peace et al., 2017). Lastly, lateral fire channeling (LFC) results in the fire propagating mostly perpendicular to the wind direction, often with spot fires, under the circumstance of steep slope and abundant fuel load in forest vegetation (J. Sharples et al., 2011, 2017). LFC forms due to interaction of wind shear on steep slopes and has already been identified in various locations such as California in USA, Sardinia in Italy, Portugal, Canberra and Blue Mountains in Australia since 2003 (J. Sharples et al., 2011). LFC requires both topographical and vegetational elements. Favorable terrain to cause LFC is a steep and lee-facing slope, while the required vegetation type is forest with heavy fuel load. LFC can cause rapid spread and the generation and transport of fire brands (J. Sharples et al., 2011).

We simulate fire propagation between three fire isochrones treated as observed data. Firstly, the fire is simulated without considering fire suppression from the initial ignitions in a large-scale fire isochrone. Then the valley, which was indeed burnt according to observed data, is focused on by using smaller fire simulations to identify the type of dynamic wind present by comparing simulated to observed spread under different wind parameterizations. Methods employed include (1) Prototype 2, which is a fire simulator developed based on Australia Fire Danger Rating System (AFDRS) specification (Ozaki et al., 2022), (2) wind vector maps with two types of surface wind fields, (3) numerical weather model vertical sounding charts (NWMVS). Prototype 2 functions not only as a fire simulator but also to identify lateral fire channeling (LFC) through the incorporation of a new

 doi:10.20944/preprints202307.1502.v1

terrain filter function. The wind vector maps provide a large-scale, dynamic view of wind interaction with terrain and vegetation. NWMVSs demonstrate various weather components such as wind vector and temperature. NWMVSs also help identify dynamic wind by plotting temporal changes of weather, such as temperature and wind. Forced channeling (FC) and lateral fire channeling (LFC), both of which can enforce the fire propagation, are hypothesized to take place because the fire spread rapidly through the valley compared to the observed fire isochrones. Although the fire simulator takes into account the weather conditions such as temperature and relative humidity, the observed fire appeared to spread faster than the simulation. Atypical wind, which the simulator does not include, could have an impact on the observed fire.

2. Study Area, Dataset and Methodology

2.1. Spatial coordinate system and datetime, study area and spatial dataset

Some spatial datasets are employed as parameters for fire simulator, Prototype 2, and weather plots, and as the observed data to verify the quality of fire simulation.

Spatial coordinate system and datetime

The coordinate system and time zone to represent in this study area follow GDA94 zone 55 and local time (Australia/Hobart) with "yyyy-MM-dd" format respectively unless mentioned explicitly. The study area is the Gell River Fire which is characterized by rugged terrain and abundant buttongrass moorland. The modelling domain in that coordinate system was defined to extend beyond the mapped boundary of the Gell River Fire (Figure 1).

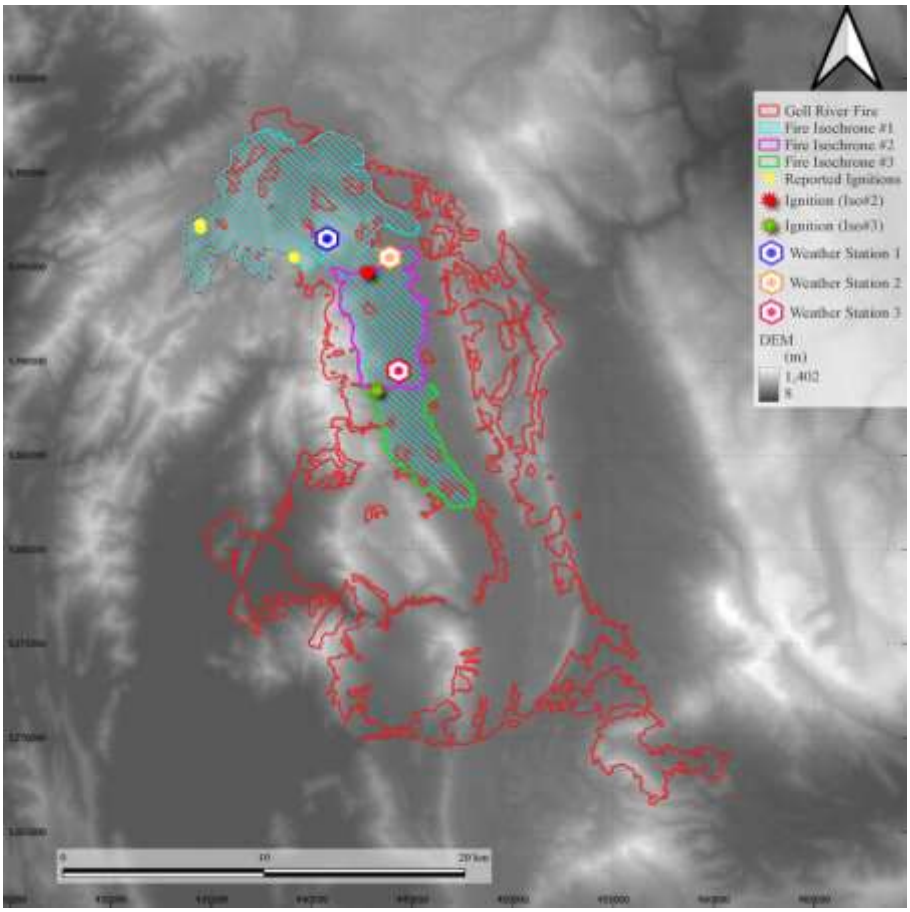

Figure 1. Extent of geospatial parameters for the Gell Fire with fire isochrones, #1 in hashed blue, #2 in magenta and #3 in light green. Some ridges are more than 1 km elevation above sea level. There are two types of ignitions employed in the simulation initialization, one is the fire start location reported by Tasmanian Fire Service (TSF) shown as a yellow circular icon, while transit ignitions, marked with

 doi:10.20944/preprints202307.1502.v1

red or green stars, are intermediate initialization points representing the assumed location of the fire from the preceding isochrone at the border. Therefore, ignition time on #2 and #3 carries over from the ending time of the previous isochrone. There are three pseudo weather stations employed for meteorological analysis. One is represented in blue honeycomb icon on the ridge (838m). The second is denoted in a yellowish honeycomb icon on the valley axis (503m). The third is in a red honeycomb on the valley axis (514m).

Study fire

The study area is characterized by ruggedness and moorland. We quantify ruggedness using the standard deviation of digital elevation model (DEM) within the study site. Although the Riveaux Road Fire, which is one of three large fires in the same season, was much larger, 637 km^2, than the Gell River Fire, 350 km^2, standard deviation of DEM, which represents ruggedness in our study, in the Gell River Fire is greater, 156.28 m than the other, 142.15 m (Geoscience Australia, 2020; Ozaki et al., 2022). This study focuses on three isochrones: #1, #2 and #3, in which the elevation gap between the highest and lowest points is 619 m, 603 m and 500 m respectively. The combination of vegetation present is suitable for rapid fire spread. Moorland, including buttongrass, accounts for 43.19% and 18.53% in the Gell River and Riveaux Road Fire respectively. Forest type, which is one of requirements of lateral fire channeling (LFC), is also abundant (35.62%) in the Gell River (Land Information System Tasmania, 2020; J. Sharples et al., 2011, 2017). All three isochrones also contain moorland groups, which account for more than half of all vegetation and possibly carry the fire to other vegetation easily, and forest type, which comprises more than one-quarter (Marsden-Smedley et al., 2001). Details of ruggedness and vegetational components are further addressed in section 1 in Appendix A.

As mentioned above, all three isochrones are employed as observed data. Isochrone #1 encloses other two smaller isochrones. Therefore, the fire in #1 lasted the longest (Table 1).

Table 1. Fire period and area in isochrones.

Isochrone	Start	End	Duration (days)	Area (km^2)
1	2018/12/28 14:25:17	2019/01/04 13:18:22	6.95	97.24
2	2019/01/04 08:05:39	2019/01/04 12:03:09	0.16	23.27
3	2019/01/04 12:03:09	2019/01/04 13:18:22	0.05	16.28

The area of isochrone #1 is nearly 100 km^2 with several reported potential ignition sites recorded by the Tasmanian Fire Service (TFS), and one of these was the starting point of the entire fire. This large isochrone is, therefore, expected to exhibit a whole picture of how the fire initially propagated in the study area. However, the overall accuracy of the fire simulation is not expected to be high because of presence of significant fire suppression activity, the location of which has not been recorded in detail, in the beginning of fire, but which was anecdotally focused around protecting fire-sensitive vegetation communities on the western flank of the fire around Lake Rhona, and commercial forestry land on the eastern flank. On the other hand, isochrone #2 and #3 are expected to identify dynamic wind and accuracy of the fire simulation because they are smaller in size than #1 while the fire could diverge larger in #1. Note that fire suppression was reportedly prepared around the ridge of the west side of #2 and #3 although it is not evident that how much was this effort conducted. The locations of fire ignitions in isochrone #2 and #3 were configured at the beginning of each isochrone. Although the fire propagates with not points but fire front line, we configured single ignition point at the border of each isochrone by accounting for wind direction and vegetation distribution due to the limitation of the fire simulator.

BARRRA-TA weather datasets and downscaled wind field

Preprints (www.preprints.org) | NOT PEER-REVIEWED | Posted: 21 July 2023 doi:10.20944/preprints202307.1502.v1

This study uses the Bureau of Meteorology Atmospheric high-resolution Regional Reanalysis for Australia for the Tasmanian region (BARRA-TA) which models a range of atmospheric pressure levels and consists of various weather parameters, such as cloud coverage, precipitation, atmospheric pressure at mean sea level, temperature, dew point temperature, geopotential height, soil moisture, relative humidity (Eizenberg et al., 2021; Su et al., 2019). These parameters are employed to parameterize the Prototype 2 fire simulator, and to produce wind vector maps and numerical weather model vertical soundings (NWMVS).

Two types of surface wind fields, each of which is presumed to flow 10 meters above the ground surface, are ingested by Prototype 2. Resolutions of BARRA-TA surface wind field and the downscaled wind field are 1500 m and 356 m respectively, shown in wind vector map (Figure 2).

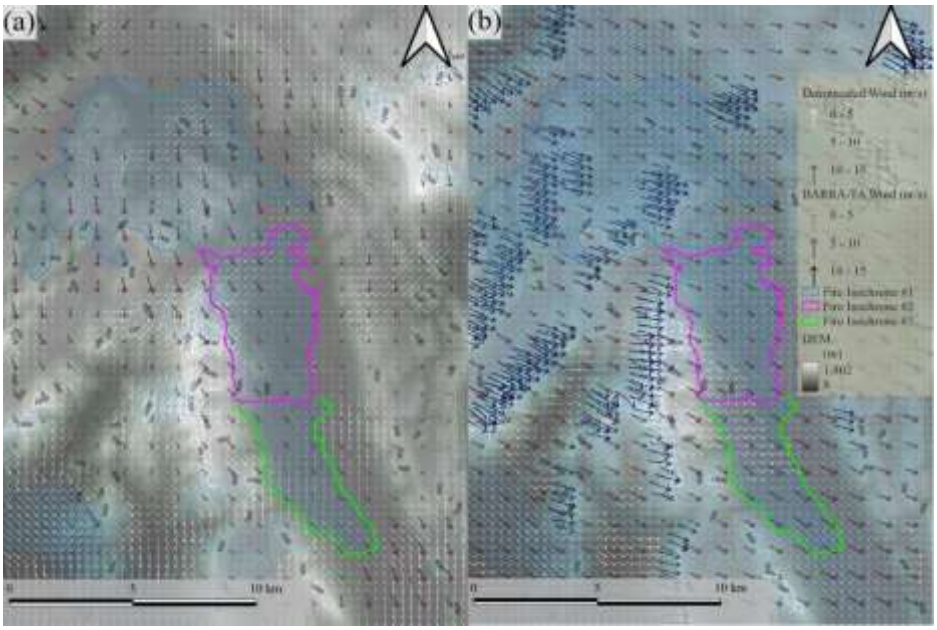

Figure 2. Wind vector map shows comparison of two types of wind field vectors both of which were captured time (a) when the fire entered in isochrone #2 in magenta and (b) when the fire entered in isochrone #3 in light green.

The wind field downscaled by WindNinja 3.7.3, which is a diagnostic tool, is more topographically sensitive than the BARRA-TA surface wind field (Firelab, 2020; Wagenbrenner et al., 2016). This wind field can also take into account the diurnal wind effect. Consequently, the downscaled wind field is approximately 16 times as fine as the BARRA-TA wind field and reflects the impact of more fine-scaled topographical features than BARRA-TA. On the other hand, an advantage of the BARRA-TA surface wind field over the downscaled wind is the inclusion of synoptic wind. Although the BARRA-TA wind field is ingested in the processing of the downscaled wind field, the synoptic component in the result data is diluted for the sake of topographical sensitivity. In fact, conducive wind structure, which is defined as the combination of wind and temperature layers and often enhances surface wind, was found to be better reflected with BARRA-TA wind field than with the downscaled wind according to the previous study (Ozaki et al., 2022).

2.2. Methods

Weather is analyzed by interpretation of both wind vector maps and weather model vertical soundings (NWMVS) while fires are simulated by Prototype 2 with terrain filter to identify the possibility of lateral fire channeling. The simulated fires are then verified using fractions skill score (FSS) to show the gap between the simulation and observation. The gap is expected to provide clues of atypical winds and lateral fire channeling (LFC), which have not been implemented in prototype 2 yet.

Preprints (www.preprints.org) | NOT PEER-REVIEWED | Posted: 21 July 2023 doi:10.20944/preprints202307.1502.v1

Wind vector map and numerical weather model vertical sounding (NWMVS)

The presence of dynamic wind is identified by interpretation of two types of plots: a wind vector map and numerical weather model vertical sounding (NWMVS). The wind vector map consists of two types of near ground surface wind fields, namely, BARRA-TA wind and downscaled wind (Figure 2). Winds at various atmospheric pressure levels are diagnosed with other weather parameters in a time series using numerical weather model vertical sounding plots (NWMVS). The target parameters for interpretation are wind direction (degrees) and magnitude (ms^{-1}), temperature (^oC), dew point temperature (^oC) and cloud coverage (%). Both wind direction and wind magnitude are available at various atmospheric pressures (hectopascal or hPa) while both temperatures were reanalysis data for near ground surface level. Note that wind at 850 hPa is referred as a geostrophic wind by following convention in this study (Whiteman & Doran, 1993). The downscaled wind also exhibits in the wind plots. NWMSV plots are only used for isochrone #2 and #3 due to the focus on dynamic winds in the valley. The weather data are plotted from three locations (Figure 2). The first is represented by blue honeycomb on the ridge near isochrone #2 (

Fig. 1) and its elevation is 858 m so that sharp drop of dew point temperature can be identified in case of downslope wind (DW). The second is in yellow honeycomb at the beginning of isochrone #2 (Fig. 1) and the valley axis with its elevation 503 m to identify forced channeling (FC). The third is in red honeycomb at the end of isochrone #2 (Fig. 1) and the valley axis with its elevation 514 m.

Fire simulator, Prototype 2 with terrain filter

Prototype 2 is an integrated fire simulator with several fire models that has been employed in a previous study of the 2019 Tasmanian fires (Ozaki et al., 2022), and has been extended in this study to include calculation of lateral fire channeling (LFC) potential via a terrain filter. The LFC is a rapid fire spread transverse to both synoptic wind and downslope wind, caused by an interaction of horizontal vortex and a lee-slope fire (J. Sharples et al., 2011, 2017; J. J. Sharples et al., 2012), which can promote localized extreme fire behavior. There are several requirements for this channeling to occur based on slope, wind speed, and vegetation type burning.

$$\gamma_s \geq \sigma \tag{1}$$

γ_s specifies topographical slope while γ is a configured threshold, which is substituted 10.5^o.

$$|\theta_w - \gamma_a| \leq \delta \tag{2}$$

θ_w is a direction of coming wind and slope aspect is represented by γ_a while δ denotes a configured threshold, which is substituted with 40^o.

$$\nu_w \geq \nu \tag{3}$$

ν_w is a speed of coming wind while ν denotes a configured threshold, which is substituted with 20 kmh^{-1}.

$$veg \in veg_f \tag{4}$$

Vegetation type (veg) must be a member of forest types (veg_f).

$$\lambda_f \geq \lambda \tag{5}$$

λ_f represents fuel load at the location as $tons\ ha^{-1}$ while λ is configured threshold, which is substituted with 15 $tons\ ha^{-1}$. The LFC is identified when all these conditions are satisfied. Note that the figures for wind speed, fuel load, fuel type and slope angle and aspect are the same as ones Sharple et al substituted (J. Sharples et al., 2017; J. J. Sharples et al., 2012).

Verification

Simulated fire propagation is verified with fire isochrones fractions skill score (FSS) (Ozaki et al., 2022). FSS evaluates the fire propagation based on a probabilistic approach by accounting for not only the cell which a cursor indicates but also grids surrounding the cell. FSS also provides "useful", which is a threshold value of the quality (Ebert, 2008; Faggian et al., 2015).

Preprints (www.preprints.org) | NOT PEER-REVIEWED | Posted: 21 July 2023 doi:10.20944/preprints202307.1502.v1

3. Results

Forced channeling (FC) was identified as influencing fire behavior by our analysis of the wind vector map and numerical weather model vertical sounding (NWMVS). On the other hand, terrain filter in Prototype 2 identified a lateral fire channeling (LFC).

3.1. Wind vector map and numerical weather model vertical sounding (NWMVS)

Synoptic wind was found to be dominant during fire period, specifically, forced channeling formed when the fire entered in the valley. Firstly, forced channeling (FC) was evident in isochrone #2 by NWMVS. When the fire entered the isochrone between 8:00 and 9:00 on 4th January 2019, BARRA-TA wind direction, denoted by the orange circle in the figure, was closer to the valley axis than the geostrophic wind at 850 hPa while downscaled wind direction was further from the valley axis than the geostrophic wind (Figure 3-a).

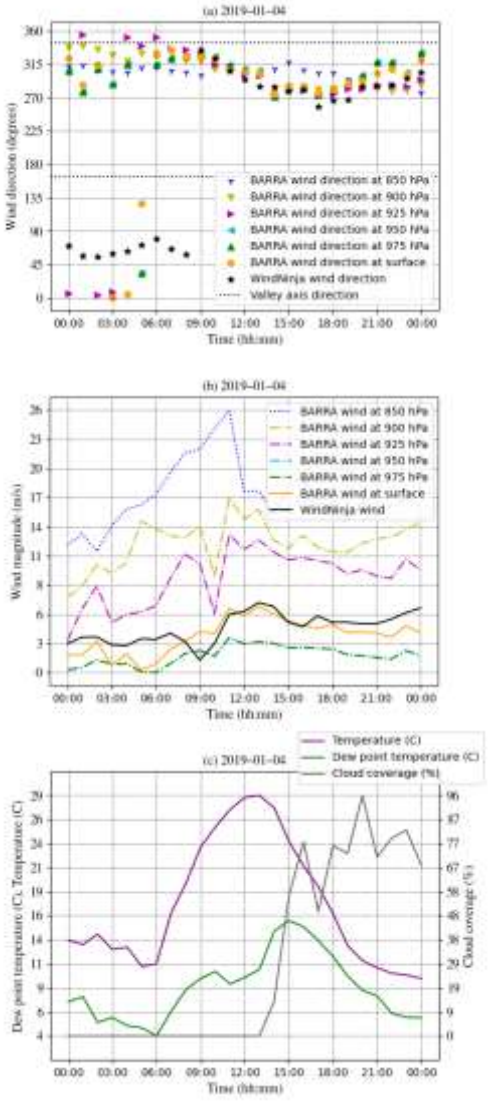

Figure 3. Wind direction (a) and magnitude (b) as well as other weather parameters (c) at pseudo weather station 2 in the valley. The presumed location recording these weather parameters is along the axis of the valley and starting point of isochrone #2. The fire started around 8 am on 4th January in 2019. Geostrophic wind (850 hPa) blew from the direction between 270 ° and 315° while both surface wind swung more by blowing between 265 ° and 360 °. Both levels winds aligned most closely when the magnitude of the geostrophic wind reaches 26 ms^{-1} at 10:00. Dew point temperature was also on the rise and reached its maximum at 13:00 on that day.

Preprints (www.preprints.org) | NOT PEER-REVIEWED | Posted: 21 July 2023 doi:10.20944/preprints202307.1502.v1

This means that the BARRA-TA wind was being refracted by terrain even though this wind field type also takes account into diurnal wind effect. Indeed, BARRA-TA can account for vertical interaction more than the downscaled wind field (Ozaki et al., 2022). FC was possible for these hours also because it tends to occur in late morning (Whiteman, 2000). On the other hand, the direction of the downscaled wind was far from the valley axis until 9:00 (Figure 3-a). This gap in direction between the two wind models could be explained by a diurnal wind effect. The diurnal wind had an impact on the downscale wind during the morning while it was replaced by synoptic wind at the entrance of the fire between 8:00 and 9:00. This tendency can be seen at pseudo weather station 1 as well (Figure 4).

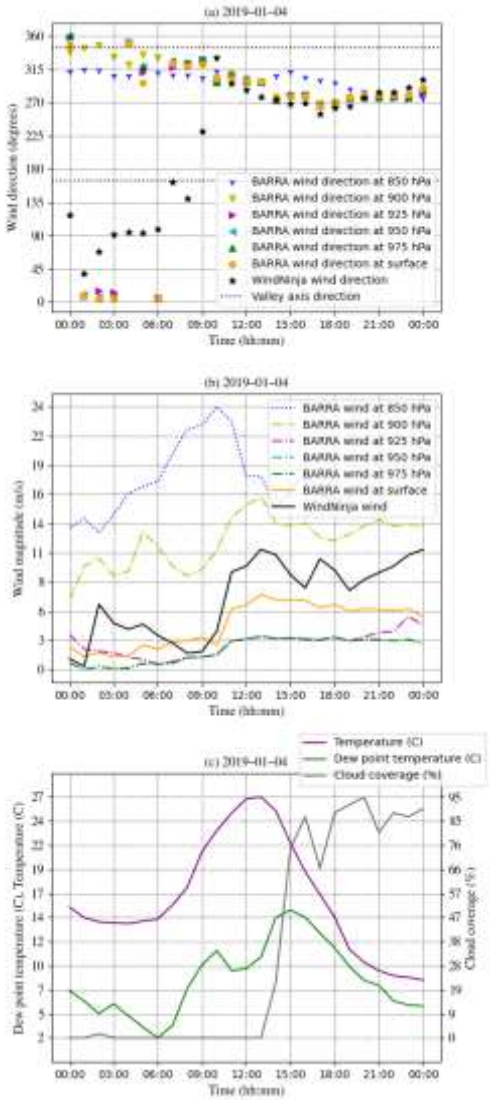

Figure 4. Wind direction (a) and magnitude (b) as well as other weather parameters (c) at pseudo weather station 1 on the ridge. The presumed location recording these weather parameters is on the ridge near isochrone #2. The fire started around 8 am on 4th January in 2019. Geostrophic wind (850 hPa) blew from the direction between 270 ° and 315° while both BARRA-TA and the downscaled surface winds swung nearly 360 ° around. All pressure levels' winds aligned when the magnitude of the geostrophic wind reaches 22 ms^{-1} at 11:00. Dew point temperature was also on the rise and reached its maximum on that day at 13:00.

The downscaled wind at station 1 on the ridge had changed its direction more frequently than station 2 in the valley. The magnitude of the downscaled wind at station 1 also increased more than the counterpart in the valley (Figure 4-a and b). This is because the air on the ridge tends to be compressed vertically and results in an increase of speed while air at lower elevations tends to relax

Preprints (www.preprints.org) | NOT PEER-REVIEWED | Posted: 21 July 2023 doi:10.20944/preprints202307.1502.v1

and decrease its speed (Whiteman, 2000). After fire entering the isochrone #2, the wind speed kept rising until 11:00 at all atmospheric pressure levels (Figure 3). After a few hours of the wind speed peak, dew point temperature reached the peak on that day in the isochrone #2 (Figure 3-c). The fire appeared to end with these two peaks because the fire duration was less than four hours in this isochrone. In other words, rapid fire spread occurred when it was dry and hot as well as while synoptic wind speed was at a maximum. During that day, the direction of the geostrophic wind was more stable than those in other pressure levels. On the other hand, the geostrophic wind gradually became less tightly coupled to the near-surface winds as its speed decreased in due course.

Secondly, the synoptic wind dominated in isochrone #3 in addition to #2. Winds in almost of all atmospheric levels were well aligned and the speed was on the rise in the valley from 8:00 till 13:00 (Figure 3-a and b and Figure 5-a and b).

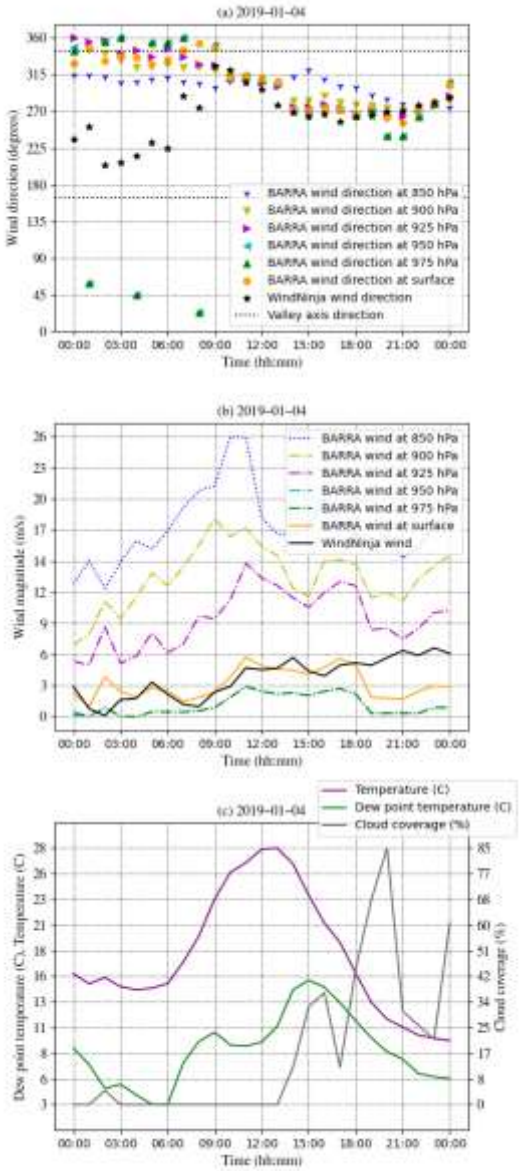

Figure 5. Wind direction (a) and magnitude (b) as well as other weather parameters (c) at pseudo weather station 3 in the valley. The presumed location recording these weather parameters is along the axis of the valley and starting point of isochrone #3. The fire started around 12:00 on 4th January in 2019. All winds including geostrophic wind (850 hPa) blew from the direction between 295 ° and 315° and aligned most closely at 12:00. Both temperature and dew point temperature were on the rise.

 doi:10.20944/preprints202307.1502.v1

The influence of synoptic wind upon surface wind was maximized when geostrophic wind reached the peak of its speed followed by increase of dew point temperature in isochrone #2 and #3 (Figure 3, Figure 4 and Figure 5).

Lastly, downslope wind was confirmed in the valley because it is at a lower elevation than ridges windward in the north and west (Figure 2-a and b). However, its effect was merely a small mitigation of wind speed because the slope angles are very small, less than 20 degrees (Figure 2-a and b). The downslope wind only functioned as a guidance of the synoptic wind into the valley as downward momentum for the forced channeling in isochrone #2 (Figure 2-a). In addition, there was no sharp drop of dew point temperature, which can often be a sign of hazardous downslope wind, at the pseudo station 1 (Figure 4-c).

3.2. Fire simulation

Simulated fires in isochrone #1 matched the coverage area well with the observed fire, while those in #2 and #3 showed the potential for lateral fire channeling (LFC) to have occurred along the valley, as well as some different fire propagation between two types of wind field used in the simulation. Firstly, fire simulations in isochrone #1 showed a mostly expected trace of fire progression. The simulated fires ignited in several locations in the highland within this isochrone (Figure 6).

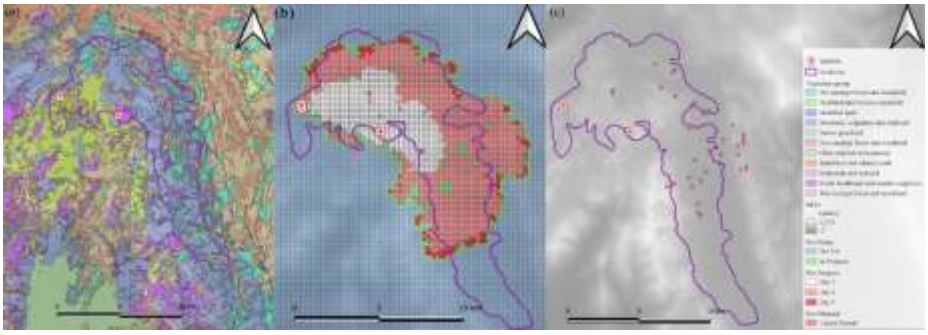

Figure 6. Vegetation group (a), fire simulation (b) and lateral fire channel (c) in isochrone #1 are shown. Lateral fire channeling exhibited mainly in the valley.

The fire then moved toward the valley in the east (Figure 6-b). There was little lateral fire channeling potential until the fire reached the valley because there was not much forest type vegetation (Figure 6-a and c). After the fire entered the valley, the potential for fire channeling was detected more frequently because not only forest but also other conditions, such as fuel load, wind speed, gap between wind direction and slope angle and aspect, were satisfied (Figure 6). Although none of simulation scores in this isochrone achieved a useful threshold, the simulated fire traced the observed fire even though the simulator did not consider the fire suppression activity. The verification scores of fire simulations are addressed in section 2, Appendix A.

Secondly, all fractions skill scores (FSS) with both wind fields were above their threshold values, 0.51, in isochrone #2 and #3. The medium FSSs are 0.69 and 0.67 with the downscaled and BARRA-TA surface wind fields respectively in isochrone #2 while they are 0.56 and 0.54 respectively in isochrone #3. Although the FSSs obtained from simulations under the two types of wind fields are close to each other, actual fire spread patterns showed slightly different propagations. The simulated fire in isochrone #2 with the downscaled wind field tended to move along the ridge on the west beyond the isochrone (Figure 7-b).

Preprints (www.preprints.org) | NOT PEER-REVIEWED | Posted: 21 July 2023 doi:10.20944/preprints202307.1502.v1

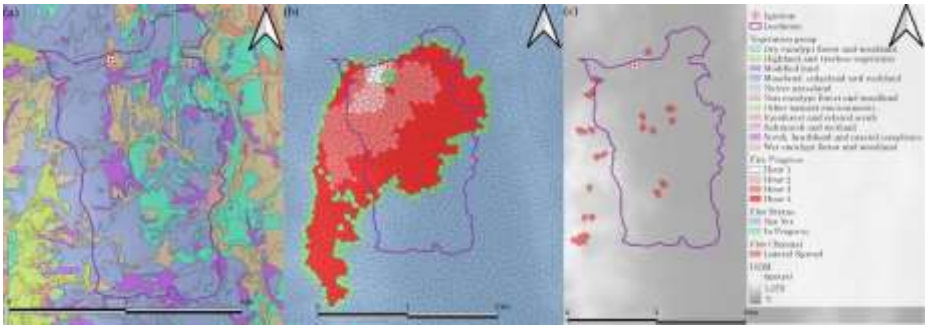

Figure 7. Vegetation group (a), fire simulation (b) and lateral fire channel (c) with downscaled wind field in isochrone #2 are shown. The simulated fire moved to the west ridge.

This ridge is the region where the fire suppression was reportedly ready to conduct. On the other hand, the simulated fire in the same isochrone with BARRA-TA wind field spread toward both east and west (Figure 8-b).

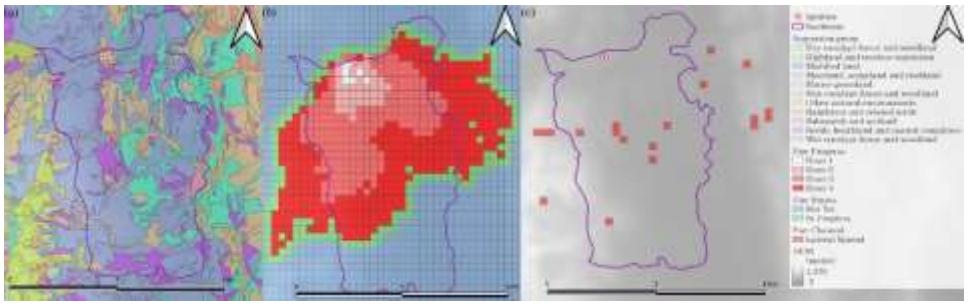

Figure 8. Vegetation group (a), fire simulation (b) and lateral fire channel (c) with BARRA-TA wind field in isochrone #2 are displayed.

Thirdly, lateral fire channeling (LFC) potential was identified in isochrone #2 and #3. The LFC areas concentrated around the valley axis with both wind field types in isochrone #2 because of abundant eucalypt forests (Figure 7-a and Figure 8-a). On the other hand, LFC was less likely to occur with the downscaled wind in isochrone #3. In effect, the lateral fire channelings (LFC) appeared less frequently with the downscaled wind than with BARRA-TA wind (Figure 9-c and Figure 10-c).

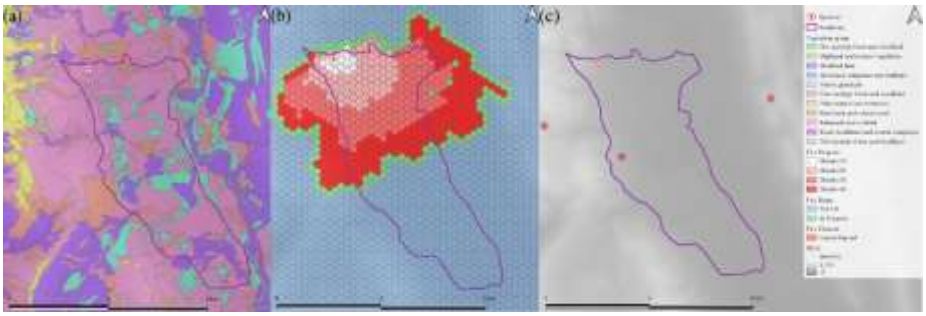

Figure 9. Vegetation group (a), fire simulation (b) and lateral fire channel (c) with downscaled wind field in isochrone #3 exhibit.

Preprints (www.preprints.org) | NOT PEER-REVIEWED | Posted: 21 July 2023 doi:10.20944/preprints202307.1502.v1

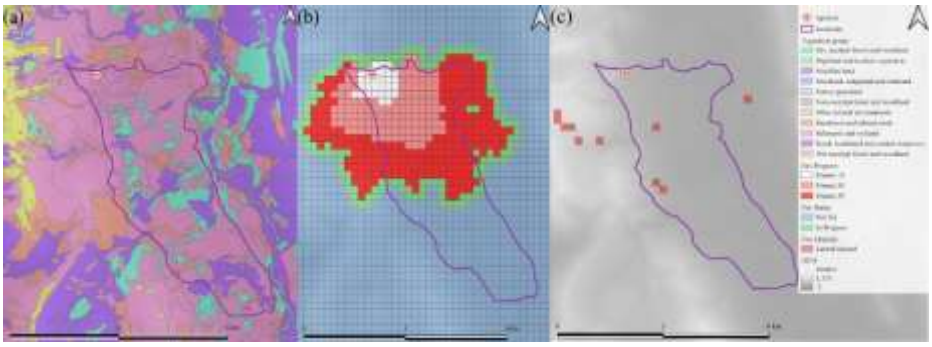

Figure 10. Vegetation group (a), fire simulation (b) and lateral fire channel (c) with BARRA-TA wind field in isochrone #3 are shown.

Conditions for LFC are the same between simulations apart from wind type. For instance, the majority of vegetation is moorland followed by eucalypt (Figure 9-a and Figure 10-a) and fire propagated wider than the isochrone in fire simulations (Figure 9-b and Figure 10-b). The wind speed was also similar in the two wind field types between 12:00 till 13:00 (Figure 5-b) while the gap of wind direction between these two fields increased (Figure 5-a). Therefore, the discrepancy of LFC is attributed to the wind direction between these two fields.

Fourthly, the simulation in #3 is less reliable than in #2 due to a few uncertainties: (1) fire suppression effort before #3, (2) possible spot fires caused by LFC in isochrone #2 beforehand and (3) lack of accuracy of the recorded fire isochrone. An example of inaccurate isochrone is that there were several unburnt regions in the final boundary in red while isochrone #3 were filled by bunt area in light green (Fig. 1). This gap is because the isochrone was estimated quickly for operational management, rather than more precisely, for research purposes.

Lastly, the observed fire spread much faster than the simulated fire. For instance, fire simulator recorded approximately 12 hours to propagate in a fire isochrone while the observed fire appeared to spend less than four hours in the isochrone. Although the fire simulator accounts for typical weather such as high temperature and low relative humidity, it does not include atypical weather phenomena such as dynamic winds. Therefore, the fire speed was adjusted in our simulations. This highlights the value of efforts to include atypical winds in future simulations.

4. Discussion and Conclusion

This study confirms the influence of forced channeling (FC) and lateral fire channeling (LFC) in the Gell River Fire. Firstly, the forced channeling (FC), which is modified synoptic wind by terrain atypically, was present for a few hours when the fire entered the valley between 8:00 and 9:00 (**Figure 3**). Fortunately, the discrepancy between surface winds and geostrophic wind was not wide, around 45°, and their gap became smaller as the geostrophic wind sped up to its maximum on that day. In terms of wind field types, BARRA-TA wind field represented FC better than the downscaled wind field (Figure 3). This might be because forced channeling is a type of modified synoptic wind and BARRA-TA wind field can take into account the vertical atmospheric interaction more than with the downscaled wind before the fire entering isochrone #2 (Ozaki et al., 2022). Yet there was no difference between them after the fire entering isochrone #2 in both weather plots and fire simulations. This is because the geostrophic wind dominated wind flow through the valley (Figure 3).

Secondly, the potential for lateral fire channeling (LFC) appeared frequently in various locations within isochrone #2 while the fire did not reach the southern end of the isochrone. A potential reason is that the LFC potential can only be identified as likely to occur but cannot yet be implemented to affect simulated fire spread. Therefore, neither fire speed nor fire spotting generation is affected by the LFC in the simulation. If these had been implemented, the simulated fire would have likely moved more southerly by lateral spreading to the south and spotting fire. A unique phenomenon regarding LFC in this study is the spread of fire between vegetation types. Mosaic or heterogeneity of vegetation is often considered as a factor reducing fire spread, however, buttongrass, which can

spread fire easily and pass it to another vegetation type, can cause vicious cycle of rapid fire spread, in combination with forest, terrain and wind.

There were some potential factors to increase uncertainty or error. The first is fire suppression activity. Reportedly, the suppression activity was prepared on the ridge of west side of the valley near isochrone #2 and #3. This activity made some difference from fire simulations. In other words, highly fire-sensitive vegetation on the west of the valley was successfully protected by fire crews. Because of the suppression activity near isochrone #2, the subsequent simulation of fire in #3 became less reliable. The third factor is the locations of ignitions in #2 and #3. The fire frontline in these isochrones was continuous and ideally it should be simulated with linear initiation in each isochrone, yet the simulations started at single point in the front line in each isochrone due to the limitation of fire simulator. The fourth is soil moisture which can affect fire simulation indirectly. This index is related to drought factor ingested by fire models while it lacked accuracy especially in the area where there are heterogeneous landcovers (Peng et al., 2017). The fifth is fire coalescence, in which the fire intensity increases when more than one fires merge. Fire isochrone #1 falls on this case, however, it was used only to glance at large picture. Other limitations are the same as previous study (Ozaki et al., 2022).

Author's contribution: Grand design: Mitsuhiro Ozaki, Grant J. Williamson. Cartography: Jagannath Aryal. Meteorology: Paul Fox-Hughes, Peter T. Love. Ecology: Grant J. Williamson. Preparation of meteorological datasets: Peter T. Love. Provision of satellite datasets: Grant J. Williamson. Implementation of method: Mitsuhiro Ozaki. Experiments: Mitsuhiro Ozaki, Grant J. Williamson. Analyzed the results: Mitsuhiro Ozaki, Grant J. Williamson, Paul Fox-Hughes, Peter T. Love, Jagannath Aryal. Wrote the manuscript: Mitsuhiro Ozaki, Grant J. Williamson, Paul Fox-Hughes, Peter T. Love, Jagannath Aryal.

Funding: The authors declare no funding.

Ethics approval and consent to participate: Not applicable.

Consent for publication: Not applicable.

Availability of data and materials: TasVeg 4 and fire history are available at Land Information System Tasmania (LIST) https://www.thelist.tas.gov.au/app/content/home) https://www.thelist.tas.gov.au/app/content/home (accessed on 19 August 2020). Curing data are available at Australian Bureau of Meteorology http://opendap.bom.gov.au:8080/thredds/catalog/curing_modis_500m_8-day/aust_regions/tas/tiff/catalog.html (accessed on 14 June 2020). DEM and Geology data are available at https://www.ga.gov.au/ (accessed on 6 February 2021). Relative Soil Moisture is available at https://eo-data.csiro.au/projects/awap/ (accessed on 26 July 2020). BARRA is available at National Computational Infrastructure (NCI) at https://nci.org.au/ (accessed on 22 May 2023). Lightning strikes or Fire Isochrone are not available in public for free. Visible Infrared Imaging Radiometer Suite (VIIRS) is available at https://www.earthdata.nasa.gov/learn/find-data/near-real-time/firms (accessed 13 November 2020). Hotspots of P-Tree system provided by JAXA is available at https://www.eorc.jaxa.jp/ptree/ (accessed 30 August 2022).

Acknowledgement: We would like to express the deepest appreciation and respect to the fire crews, operators and corresponding staff regarding the Gell River Fire.

Competing interests: The authors declare no conflict of interest.

References

1. Abouali, A., Viegas, D. X., & Raposo, J. R. (2021). Analysis of the wind flow and fire spread dynamics over a sloped–ridgeline hill. *Combustion and Flame*, *234*, 111724. https://doi.org/10.1016/j.combustflame.2021.111724
2. American Meteorological Society. (2020, April 5). *Meteorology Glossary*. http://glossary.ametsoc.org/wiki

3. Australasian Fire and Emergency Service Authorities Council. (2019, July 1). *AFAC Independent Operational Review: A review of the management of the Tasmanian fires of December 2018—March 2019*. https://www.fire.tas.gov.au/userfiles/AFAC/AFAC_Review.pdf
4. Blackwood, G., Hardy, A., Dodd, B., Ooi, C. S., & Williams, K. (2023). Natural disaster on Instagram: Examining representations of the 2018–2019 Tasmanian fires. *Annals of Tourism Research Empirical Insights*, *4*(1), 100082. https://doi.org/10.1016/j.annale.2022.100082
5. Bowman, D. M. J. S., Kolden, C. A., & Williamson, G. J. (2022). Bushfires in Tasmania, Australia: An Introduction. *Fire*, *5*(2). https://doi.org/10.3390/fire5020033
6. Bradstock, R. A. (2010). A biogeographic model of fire regimes in Australia: Current and future implications. *Global Ecology and Biogeography*, *19*(2), 145–158.
7. Ebert, E. E. (2008). Fuzzy verification of high-resolution gridded forecasts: A review and proposed framework. *Meteorological Applications*, *15*(1), 51–64.
8. Edalati-nejad, A., Ghodrat, M., & Simeoni, A. (2021). Numerical Investigation of the Effect of Sloped Terrain on Wind-Driven Surface Fire and Its Impact on Idealized Structures. *Fire*, *4*(4), 94. https://doi.org/10.3390/fire4040094
9. Eizenberg, N., Jakob, D., Fox-Hughes, P., Steinle, P., White, C., & Franklin, C. (2021). BARRA v1.0: Kilometre-scale downscaling of an Australian regional atmospheric reanalysis over four midlatitude domains. *Geoscientific Model Development*, *14*, 4357–4378. https://doi.org/10.5194/gmd-14-4357-2021
10. Faggian, N., Roux, B., Steinle, P., & Ebert, B. (2015). Fast calculation of the fractions skill score. *Mausam*, *66*(3), 457–466.
11. Firelab. (2020, May 13). *WindNinja Tutorials version 3.6.0*. WindNinja Tutorials Version 3.6.0. https://weather.firelab.org/windninja/tutorials/
12. Geoscience Australia. (2020, May 23). *Geoscience Australia*. https://www.ga.gov.au/
13. Heilman, W. E. (2023). Atmospheric turbulence and wildland fires: A review. *International Journal of Wildland Fire*. https://doi.org/10.1071/WF22053
14. Hydro Tasmania. (n.d.). *Gordon-Pedder*. Retrieved January 18, 2023, from https://www.hydro.com.au/clean-energy/our-power-stations/gordon-pedder
15. Kossmann, M., Sturman, A., & Zawar-Reza, P. (2001). *Atmospheric influences on bush fire propagation and smoke dispersion over complex terrain*.
16. Land Information System Tasmania. (2020, May 18). *LISTMap*. http://maps.thelist.tas.gov.au/listmap/app/list/map
17. Marsden-Smedley, J. B., Catchpole, W. R., & Pyrke, A. (2001). Fire modelling in Tasmanian buttongrass moorlands. IV. Sustaining versus non-sustaining fires. *International Journal of Wildland Fire*, *10*(2), 255–262.
18. Ozaki, M., Harris, R. M. B., Love, P. T., Aryal, J., Fox-Hughes, P., & Williamson, G. J. (2022). Impact of Vertical Atmospheric Structure on an Atypical Fire in a Mountain Valley. *Fire*, *5*(4). https://doi.org/10.3390/fire5040104
19. Peace, M., Mccaw, L., Santos, B., Kepert, J. D., Burrows, N., & Fawcett, R. J. (2017). Meteorological drivers of extreme fire behaviour during the Waroona bushfire, Western Australia, January 2016. *Journal of Southern Hemisphere Earth Systems Science*, *67*(2), 79–106.
20. Peng, J., Loew, A., Merlin, O., & Verhoest, N. E. C. (2017). A review of spatial downscaling of satellite remotely sensed soil moisture. *Reviews of Geophysics*, *55*(2), 341–366. https://doi.org/10.1002/2016RG000543
21. Sharples, J. J. (2009). An overview of mountain meteorological effects relevant to fire behaviour and bushfire risk. *International Journal of Wildland Fire*, *18*(7), 737–754.
22. Sharples, J. J., McRae, R. H. D., & Wilkes, S. R. (2012). Wind–terrain effects on the propagation of wildfires in rugged terrain: Fire channelling. *International Journal of Wildland Fire*, *21*(3), 282–296.
23. Sharples, J. J., Mills, G. A., McRae, R. H., & Weber, R. O. (2010). Foehn-like winds and elevated fire danger conditions in southeastern Australia. *Journal of Applied Meteorology and Climatology*, *49*(6), 1067–1095.
24. Sharples, J., Richards, R., Hilton, J., Ferguson, S., Cohen, R., & Thatcher, M. (2017). *Dynamic simulation of the Cape Barren Island fire using the Spark framework*. 1111–1117.
25. Sharples, J., Viegas, D., McRae, R., Raposo, J., & Farinha, H. (2011). *Lateral bushfire propagation driven by the interaction of wind, terrain and fire*. 235–241.
26. Simeoni, A., Salinesi, P., & Morandini, F. (2011). Physical modelling of forest fire spreading through heterogeneous fuel beds. *International Journal of Wildland Fire*, *20*(5), 625–632.
27. Smedman, A.-S., Bergström, H., & Högström, U. (1996). Measured and modelled local wind field over a frozen lake in a mountainous area. *Contributions to Atmospheric Physics 69*, 501–516.
28. Storey, K. (2010). *A review of the potential interactions between fire, soil, hydrology and geomorphology of buttongrass moorland*. 10.
29. Su, C.-H., Eizenberg, N., Steinle, P., Jakob, D., Fox-Hughes, P., White, C. J., Rennie, S., Franklin, C., Dharssi, I., & Zhu, H. (2019). BARRA v1. 0: The bureau of meteorology atmospheric high-resolution regional reanalysis for Australia. *Geoscientific Model Development*, *12*(5), 2049–2068.

30. Turner, P. A. M., Balmer, J., & Kirkpatrick, J. B. (2009). Stand-replacing wildfires?: The incidence of multi-cohort and single-cohort Eucalyptus regnans and E. obliqua forests in southern Tasmania. *Old Forests, New Management: The Conservation and Use of Old-Growth Forests in the 21st Century*, *258*(4), 366–375. https://doi.org/10.1016/j.foreco.2009.04.021
31. Wagenbrenner, N. S., Forthofer, J. M., Lamb, B. K., Shannon, K. S., & Butler, B. W. (2016). Downscaling surface wind predictions from numerical weather prediction models in complex terrain with WindNinja. *Atmospheric Chemistry and Physics*, *16*(8), 5229–5241.
32. Whiteman, C. D. (2000). *Mountain meteorology: Fundamentals and applications*. Oxford University Press: New York, USA,.
33. Whiteman, C. D., & Doran, J. C. (1993). The relationship between overlying synoptic-scale flows and winds within a valley. *Journal of Applied Meteorology*, *32*(11), 1669–1682.